Material contrast in scanning near-field optical microscopy at 1–10 nm resolution

J. Koglin, U. C. Fischer,* and H. Fuchs
Physikalisches Institut, Westfälische Wilhelms-Universität, Wilhelm-Klemm-Straße 10, D-48149 Münster, Germany
(Received 13 September 1996)

The tetrahedral tip is used as a light emitting probe for scanning near-field optical microscopy (SNOM). It has no aperture as an element for the confinement of light and the techniques of scanning tunneling microscopy and SNOM can be combined with the same probing tip. Silver grains are distinguished from gold grains by their specific near-field optical contrast in SNOM transmission mode images of mixed films of silver and gold at a lateral resolution in the nanometer range and an edge resolution of 1 nm for selected grains. The contrast is explained in terms of a quasielectrostatic model of a local light-emitting source interacting with the object. [S0163-1829(97)06211-5]

I. INTRODUCTION

The diffraction-limited resolution of light microscopy can be circumvented by the technique of scanning near-field optical microscopy (SNOM), where a nanoscopic source of light is scanned in close proximity with respect to the object. The near-field interaction between the source and the object modifies the light emission of the source. This signal is used as information about optical properties of the object at a resolution that is limited by the size of the source and its distance to the object rather than by the wavelength. Small apertures in a thin metal film were introduced as a light-confining element to create a light source for SNOM.[1–5] SNOM with an aperture placed at the apex of a metal-coated tapered fiber seems to reach a resolution limit of 30 nm.[6] Without doubt there is a strong interest to push this limit further to the 1-nm scale in order to obtain information about optical properties at molecular resolution. The tetrahedral tip[7] that has no aperture as a light-confining element was introduced as a probe for SNOM to increase the resolution substantially below 30 nm.[8]

Here experiments are reported, demonstrating the performance of the tetrahedral tip in SNOM experiments on metal films of heterogeneous composition, showing that a characteristic material contrast at a resolution of 1 nm is obtained. The contrast is interpreted by a quasistatic model based on the interaction of a probing dipole with a mirror dipole induced in the object.

SNOM with the tetrahedral tip

A scheme of the tetrahedral tip is shown in Fig. 1. The bulk of this tip consists of one corner of a triangular glass fragment of a microscope cover glass. It is coated with a 50-nm-thick vacuum deposited gold film, which has a granular structure with grain sizes on the order of 20 nm, as revealed by scanning electron microscopy (SEM) micrographs.[9] Due to the oblique evaporation process,[7,8] the edge $K1$ is expected to be coated with less metal than the rest of the structure as indicated in the scheme of Fig. 1. To irradiate the tetrahedral tip from within the bulk, the fragment is attached by a transparent glue of matching refractive index onto a small prism as shown in Fig. 2. The special form of the tip was chosen with the aim that light, which is directed onto the tip, is confined to the nanometric dimensions of the apex of this tip with a concomitant strong increase in light intensity. On the basis of an experimental investigation of the optical properties of the tetrahedral tip, a hypothetical model was suggested of how this confinement might occur by compression of light in a three-step process:[10] An incoming plane wave is first transformed to surface plasmons on the side faces $S12$ and $S13$ of the tip. The surface plasmons travel towards the edge $K1$, where they are converted into a linear surface plasmon traveling along the edge towards the tip. The linear plasmon excites a local plasmon on a metal grain on the tip.

For SNOM experiments, the tetrahedral tip is incorporated in a combined SNOM/scanning tunneling microscopy (STM) setup[11] as shown schematically in Fig. 3. The light ($\lambda = 635$ nm, $h\nu = 1.95$ eV) transmitted through the sample

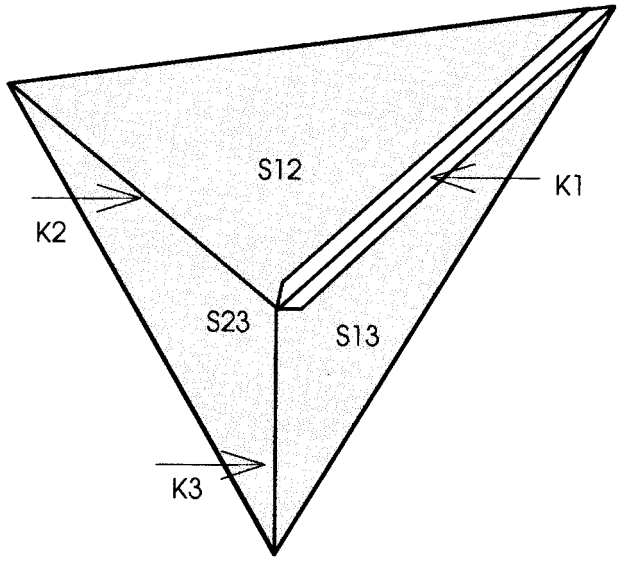

FIG. 1. Scheme of the tetrahedral tip. The faces $S12$, $S13$, and $S23$, the edges $K2$ and $K3$, and the tip are coated with gold, whereas the edge $K1$ is coated with less gold due to the oblique evaporation process.

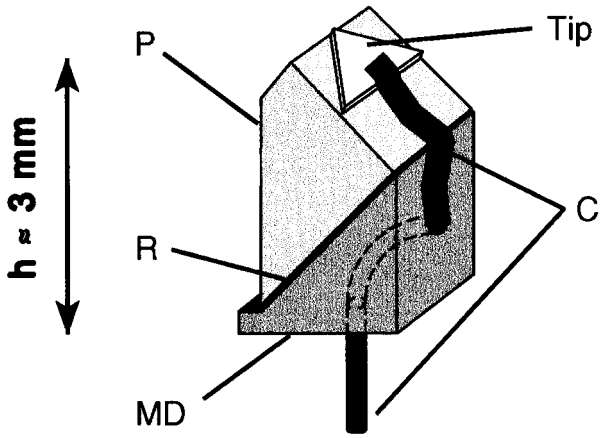

FIG. 2. Mounting of the tetrahedral tip. *P*, prism; *R*, reflecting mirror; *MD*, mounting device; *C* electrical contact.

is detected and used as a signal for SNOM. The STM feedback is used to control the distance between tip and sample during a scan and yields a topographic image of the sample simultaneously with the SNOM signal. The STM mode requires an electrically conducting sample and restricts the choice of accessible samples for SNOM with the tetrahedral tip. In first SNOM images of evaporated silver films, light-absorbing dark grains are observed with a resolution of 6 nm, indicating that the tetrahedral tip indeed acts as a nanometric light source.[11]

II. EXPERIMENTS

Metal films of heterogeneous composition were investigated by SNOM with respect to their local optical properties. When investigating an optical contrast it is preferable that the sample is very flat. Otherwise a convolution between topographic (STM-dependent) and optical contrast may lead to an only apparently high resolution in the SNOM image.

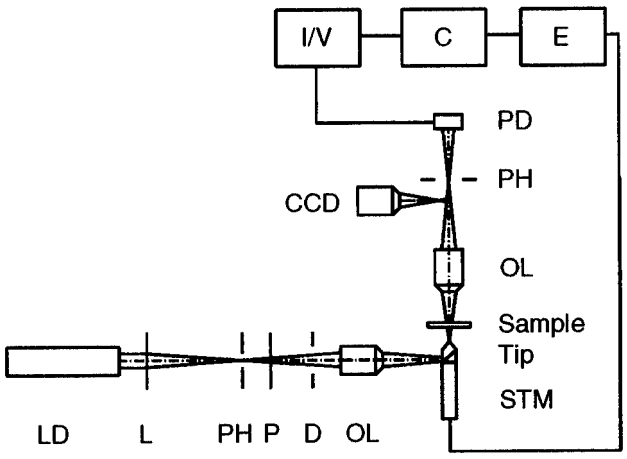

FIG. 3. Scheme of the combined SNOM/STM setup. *LD*, laser diode; *L*, lens; *PH*, pinhole; *P*, polarizer; *D*, iris diaphragm; *OL*, objective lens; *CCD*, CCD camera; *PD*, photodetector; *I/V*, current-to-voltage converter; *C*, computer; *E*, control electronics.

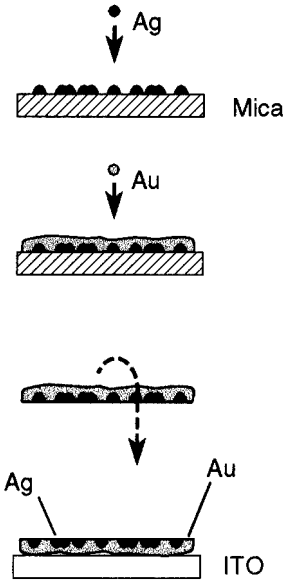

FIG. 4. Preparation of inverted mixed Ag/Au films.

For a preparation of metal films with a flat surface, a replica technique is applied where metal is evaporated onto an atomically flat piece of mica or onto float glass. The film is inverted and the now exposed surface is investigated. Three metal samples of different composition were prepared: (i) a gold film, (ii) a mixed film of gold and silver, and (iii) a projection pattern consisting of gold and silver.

A. Preparation

1. Gold film

After evaporation of a 50-nm-thick gold film onto a freshly cleaved piece of mica, the gold film was floated off onto the surface of clean water. Then the film was deposited upside down onto a piece of glass, which was covered with a 20-nm-thick film of indium tin oxide.

2. Mixed films of gold and silver

Mixed films of gold and silver were investigated in order to find out whether silver and gold grains can be distinguished in SNOM images. The mixed films were prepared as shown in Fig. 4. First 0.4 nm of silver and then 50 nm of gold were evaporated onto a freshly cleaved piece of mica. Then the film was inverted as described.

3. Projection pattern

In contrast to the mixed film, the local distribution of silver and gold is known in this sample. A 5-nm-thick latex projection pattern[12] of gold embedded into the surface of a 10-nm-thick film of silver was prepared as shown in Fig. 5. A 5-nm-thick gold film is evaporated through a mask of hexagonally close-packed latex spheres of a diameter of 0.22 μm onto a 1-mm-thick piece of float glass. The latex spheres are then removed and the projection pattern is covered with a 10-nm-thick film of silver. The composite metal film is embedded into a thin film of a polyester resin supported by a second piece of glass. By gently applying mechanical force

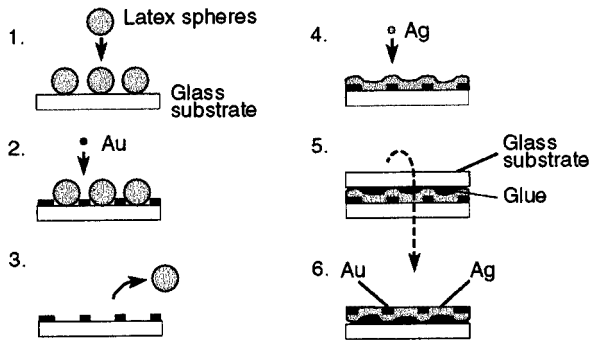

FIG. 5. Preparation of gold patterns embedded in a silver film. The process is described in the text.

between the two glass plates the first glass piece is separated from the metal film. In this way the gold projection pattern embedded into the surface of the silver film becomes exposed.

B. SNOM experiments

1. Gold film

Figures 6(a) and 6(b) show STM and SNOM images of a 50-nm-thick gold film. We expect the topography of the inverted gold film to be a replica of the atomically flat mica. The topography of the inverted film as revealed by STM has a root-mean-square surface roughness ($\sigma_{\rm rms}$) of $\sigma_{\rm rms} = 0.6$ nm as compared to $\sigma_{\rm rms} = 1.2$ nm of a noninverted film as measured with the tetrahedral tip. Also in the inverted film a granular topography of the metal film is clearly seen. We assume that during the evaporation process metal island films do not coalesce completely on the substrate such that gaps between different grains remain visible on the inverted film.

Interestingly, in the SNOM image the gold grains appear bright in their center in contrast to the previously observed silver grains appearing dark.[11] This indicates that gold grains and silver grains have a different near-field optical contrast. However, not all of the gold grains appear bright; some of them show an absorption contrast that can be seen from a comparison of the STM and SNOM images of a gold film shown in Figs. 7(a) and 7(b).

2. Mixed films of gold and silver

Figures 8(a) and 8(b) show STM and SNOM images of an inverted mixed film of gold and silver. In the topography the typical granular structure of the metal film is seen. Again the surface roughness is very small and the maximum height (peak to valley) is only 5 nm. The SNOM image shows a distinct contrast that corresponds only occasionally to the topographic image. Several grains, such as the ones labeled *a* in Figs. 8(a) and 8(b), can be identified as dark grains in the SNOM image. A line profile across such a grain [Fig. 9(a)] shows a close correspondence of these grains in the topographic STM image and the SNOM image, respectively. Other grains, labeled *b* in Figs. 8(a) and 8(b), appear homogeneous in the STM image, whereas in the SNOM image they do not appear as a homogeneous grain. A dark grain

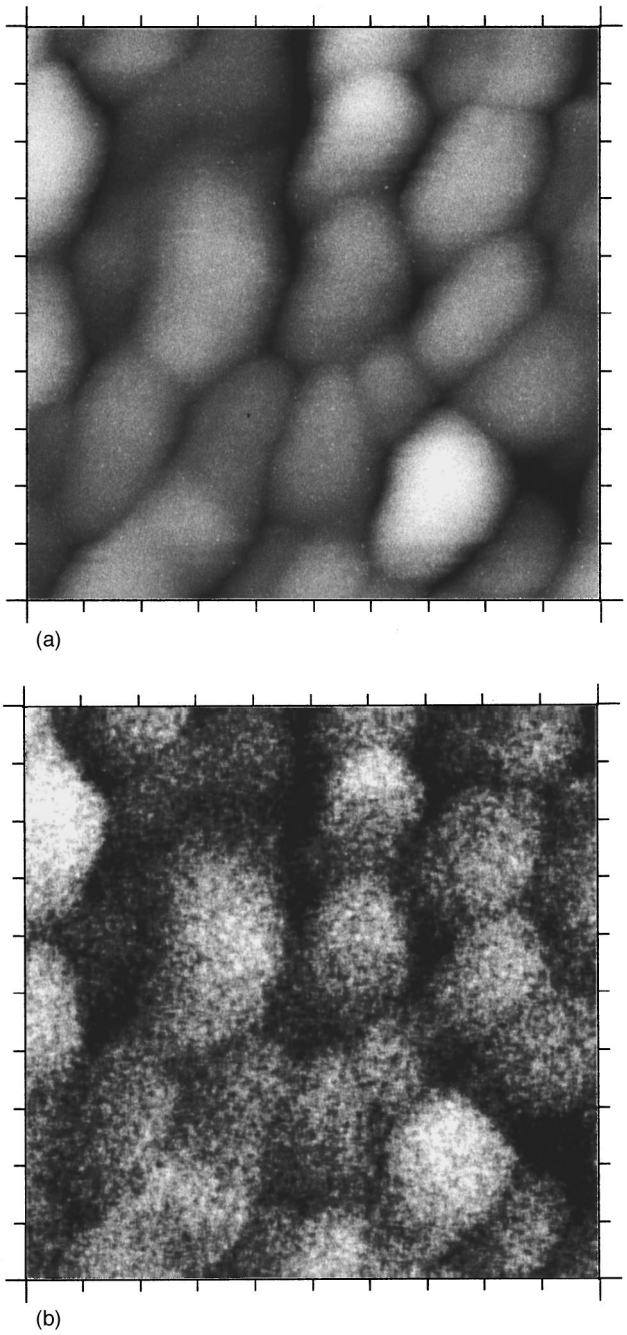

FIG. 6. Inverted gold film ($d = 50$ nm) on an ITO substrate. (a) STM image and (b) SNOM image (scan range 125×125 nm^2).

seems to be embedded in a bright surrounding grain as is again seen very clearly in a line the profiles shown in Figs. 9(b) and 9(c), which were taken in orthogonal directions as indicated in Fig. 8. The transition from 10% to 90% between the bright and dark regions within this grain is found to be as narrow as 1 nm. It is likely that some of the grains, appearing dark in the SNOM image, are silver grains for several reasons. (i) From the preparation of the films it is expected that silver grains are present. The distribution of the dark grains is qualitatively consistent with the distribution of silver grains of a 0.4-nm-thick silver island film as known from transmission electron micrographs of evaporated silver films.[13] (ii) From the SNOM images of pure silver films[11]

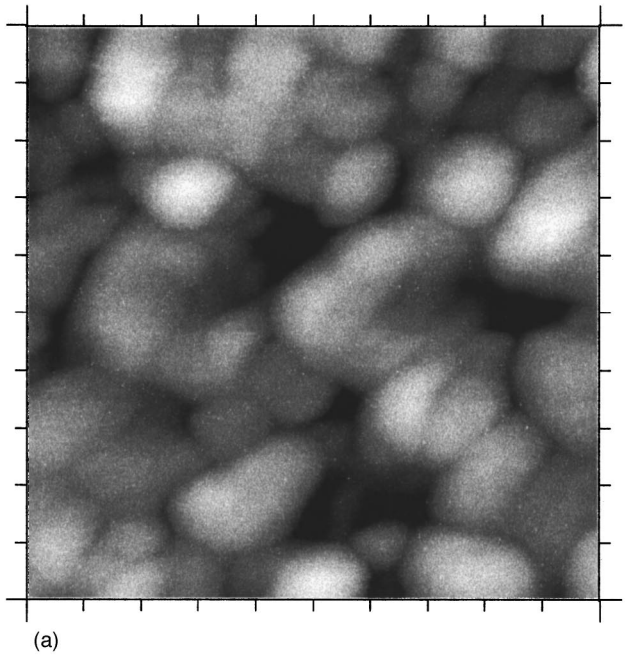

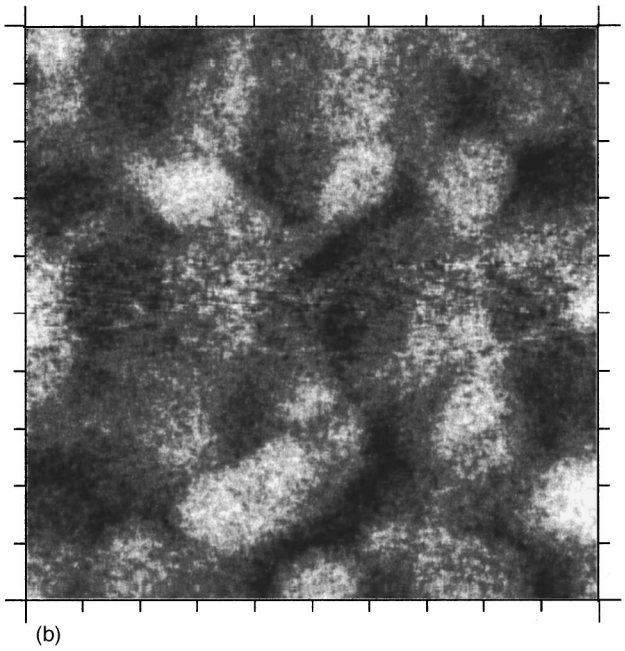

FIG. 7. Inverted gold film ($d=50$ nm) on an ITO substrate. (a) STM image and (b) SNOM image (scan range 125×125 nm^2).

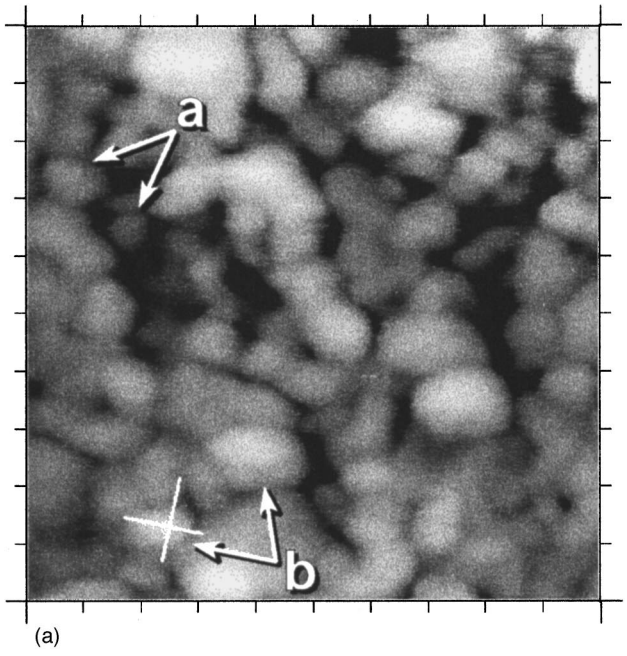

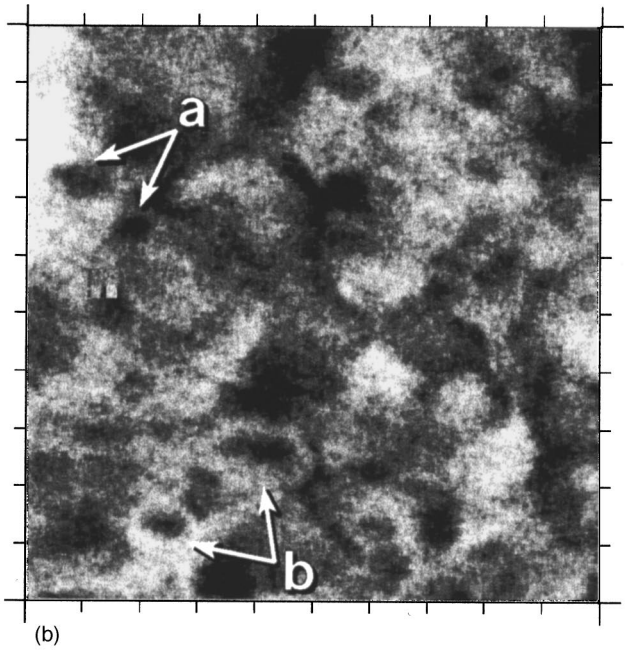

FIG. 8. Inverted mixed film of silver ($d=0.4$ nm) and gold ($d=50$ nm) on an ITO substrate. (a) STM image and (b) SNOM image (scan range 125×125 nm^2).

and of pure gold films (Fig. 6) we expect silver grains to appear dark and the majority of gold grains to appear brighter. (iii) The different types of grains labeled *a* and *b* may represent isolated and embedded silver grains, respectively, as is plausible from the preparation of the film.

Some of the type-*a* grains may represent isolated silver grains that did not coalesce with the embedding gold film, whereas others may represent gold grains that appear dark, as shown in Fig. 7(b). Type-*b* grains may correspond to silver grains embedded into a larger gold grain, where no feature can be recognized in the transition region in the topographic STM image due to a coalescence of gold and silver in the evaporation process. We conclude that these embedded type-*b* grains must be silver grains because in pure gold films grains of this type were never observed. Since in the SNOM image the transition between dark and bright regions occurs over a width of less than 1 nm [Figs. 9(b) and 9(c)], where there is no detectable topographic feature, this result implies an edge resolution of 1 nm in the SNOM image. So far, we cannot directly prove that the type-*b* grains consist of silver since it is very difficult to distinguish between silver and gold on this scale by an independent method.

3. Projection pattern

To confirm our conclusion that type-*b* grains are silver grains we investigated the projection pattern as a sample

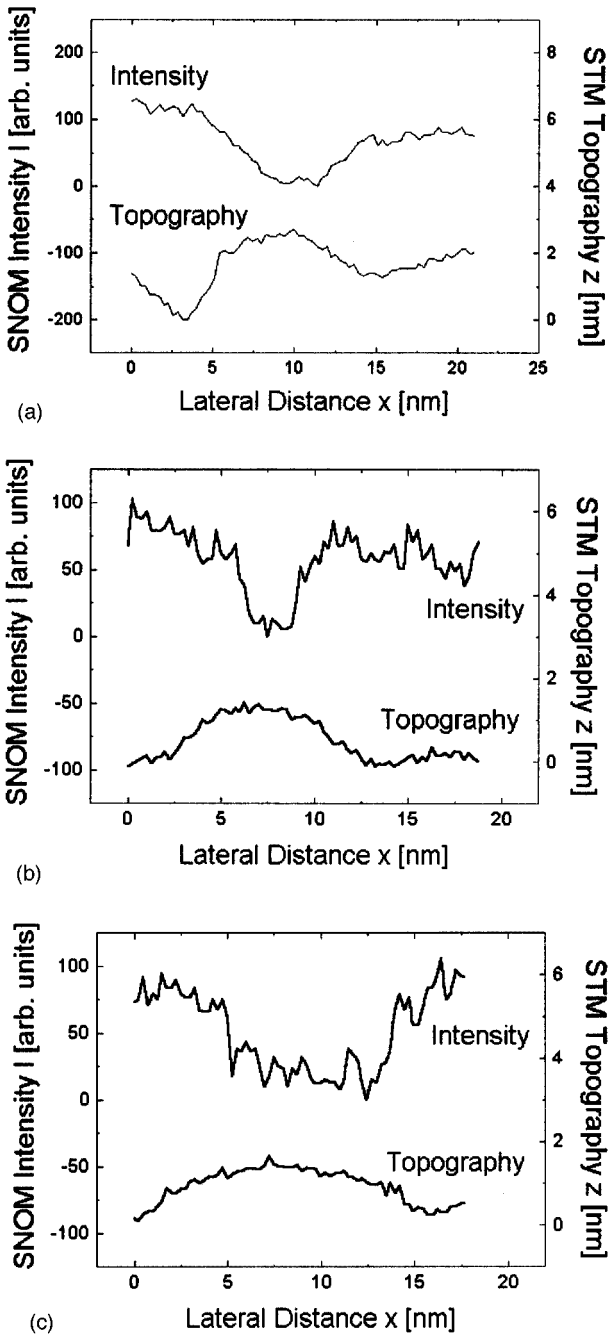

FIG. 9. Line profiles across a metal grain: (a) labeled with *a*; (b) and (c) labeled with *b* in Figs. 8(a) and 8(b). The profiles shown in (b) and (c) are taken at orthogonal directions as indicated in Fig. 8(a).

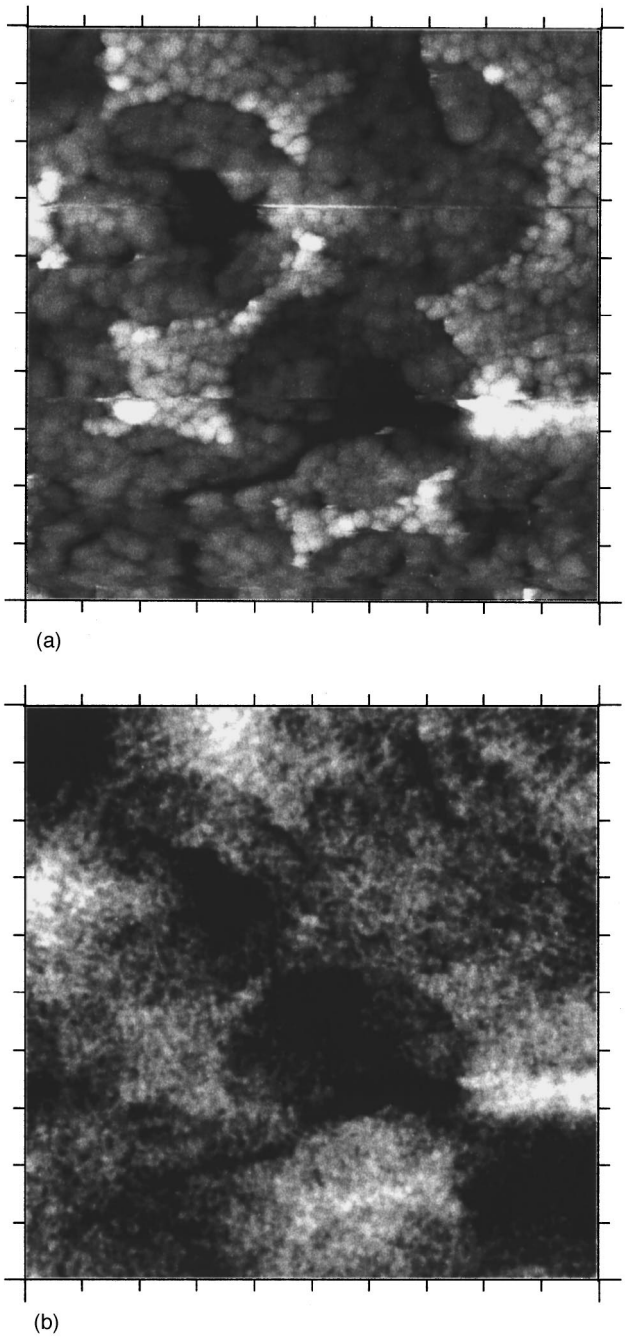

FIG. 10. Inverted gold projection patterns ($d = 5$ nm) embedded into a silver film ($d = 10$ nm). (a) STM image and (b) SNOM image (scan range 500×500 nm^2).

where the local distribution of silver and gold is known. With this sample we intend to test the different contrast of silver and gold. It is, however, not well suited to test resolution because the embedded structures are much coarser than the fine silver grains of the mixed film of gold and silver described before. STM and SNOM images of the projection pattern are shown in Fig. 10(a) and 10(b).

In the STM image the projection pattern is recognized by a slight topographic contrast of about 3 nm. Independent investigations of the same sample by atomic force microscopy confirmed this topographic contrast. The origin of this topography is not clear. A likely explanation could be that during removal of the latex spheres with organic solvent a very thin film of polymer remains on the glass substrate. These sites are therefore expected to appear as depressions in the metal replica. Also in the SNOM image the projection pattern is recognized. As a result, areas where gold is exposed at the surface appear brighter than areas where silver is exposed. These results are consistent with our interpretation of the previous SNOM images of statistically distributed silver grains embedded in a gold film.

Furthermore, we performed approach experiments at surface areas of the projection pattern where there is gold on top

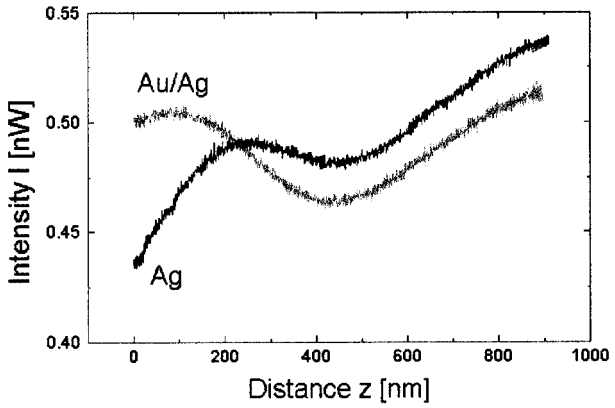

FIG. 11. SNOM signal I of the tetrahedral tip as a function of the distance z to regions where silver (Ag) or gold (Au/Ag) is exposed at the surface of the composite metal film, as shown in Fig. 10. $z=0$ is defined by the onset of the tunneling current.

of silver and at areas where there is only silver. Figure 11 shows a representative example of the SNOM signal as a function of distance between the tip and sample for two such sites. The approach was stopped with the onset of the tunneling current. The two approach curves show a different interference type of behavior. From these curves we draw the following conclusions. (i) The difference in the SNOM signal for the case of tunneling contact at sites of silver and gold accounts for the contrast of about 8% observed in the SNOM image. (ii) The onset of the tunneling contact does not lead to an abrupt change in the SNOM signal. Therefore, we can exclude that an influence of the tunneling current on the SNOM signal is the origin of the image contrast.

III. DISCUSSION

It is remarkable that the observed contrast cannot be explained by the local transmissivity of the sample. The experimentally observed transmission of a 50-nm-thick metal film is about 1% for silver and 10% for gold, respectively. Thus the transmission is expected to be smaller at sites where silver and gold are present than at sites where gold is missing, in contrast, to the observed SNOM signal in the last example of the latex projection pattern. This seemingly contradictory result could find an explanation by a specific near-field optical contrast which is determined by the material composition of a very thin surface layer of the object. The interaction of the tip with gold could lead to an enhanced resonant scattering of the probing gold tip, whereas the interaction with silver may lead to a damping of this resonant scattering. Such a resonant scattering mechanism might explain why some of the gold grains show an absorption contrast (Fig. 7). Conditions for resonant enhancement may depend on the shape of the grain as well as on its local environment and therefore may not be fulfilled for all of the gold grains.

The local variations in the SNOM signal of Fig. 8(b), displaying a resolution much smaller than the thickness of the metal film of 50 nm, could depend on a very thin surface layer of the sample. Remote regions of the sample do not contribute to the resonant scattering process and consequently lead to the observed reduction of the overall transmitted light.

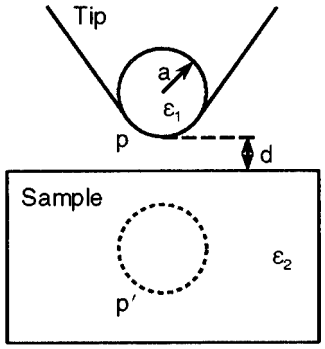

FIG. 12. Scheme of the quasielectrostatic model. ε_1, dielectric constant of the tip approximated as a sphere with radius a; ε_2, dielectric constant of the sample; d, distance between the tip and sample; p and p', the dipole moments of the sphere and of its image.

Using a quasielectrostatic model,[14–16] the observed difference in the contrast for gold and silver in the SNOM images can be understood. In this model, as shown schematically in Fig. 12, the tip is represented by a small gold sphere that is excited by an electric field E. The dipole moment p of the sphere is determined by the dielectric constant of gold ε_1 and the radius a of the sphere:

$$p=\frac{4\pi a^3}{3}\left(\frac{\varepsilon_1-1}{\varepsilon_1+2}\right)E. \tag{1}$$

The dipole p induces an image dipole p' in the sample, which depends on the dielectric constant of the sample ε_2:

$$p'=\frac{\varepsilon_2-1}{\varepsilon_2+1}p. \tag{2}$$

The electric field of the image dipole acts on the gold sphere and changes the dipole moment to an efficient dipole moment p_{eff} according to Ruppin:[17,18]

$$p_{\text{eff}}\propto\frac{\varepsilon_1-1}{4\pi+(\varepsilon_1-1)F} \tag{3}$$

with

$$F_{\parallel}=\frac{4\pi}{3}\left[1-\frac{1}{8}\left(\frac{a}{a+d}\right)^3\frac{\varepsilon_2-1}{\varepsilon_2+1}\right] \tag{4}$$

and

$$F_{\perp}=\frac{4\pi}{3}\left[1-\frac{1}{4}\left(\frac{a}{a+d}\right)^3\frac{\varepsilon_2-1}{\varepsilon_2+1}\right], \tag{5}$$

where d is the distance between the surface of the sphere and the surface of the sample. The subscripts $\parallel$ and $\perp$ indicate the orientation of the dipole moment p parallel ($\parallel$) and perpendicular ($\perp$) to the sample. We assume the SNOM signal I to be determined by the total scattering efficiency of the effective dipole moment and its effective image dipole p'_{eff}:

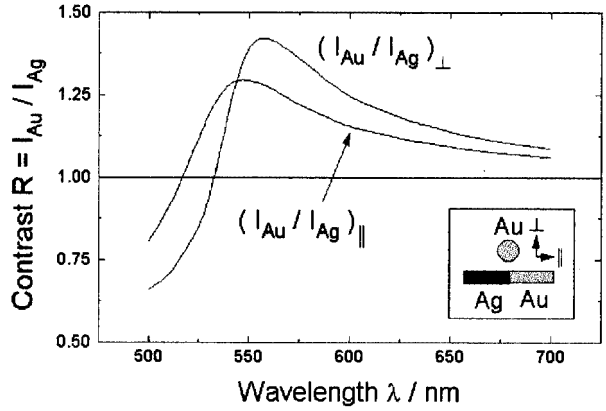

FIG. 13. Calculated ratio $R=I_{\mathrm{Au}}/I_{\mathrm{Ag}}$ of the SNOM signals I_{Au} for a sample consisting of gold and I_{Ag} for a sample consisting of silver at $d=0$. A ratio $R>1$ means that gold appears brighter than silver.

$$p'_{\mathrm{eff}}=\frac{\varepsilon_2-1}{\varepsilon_2+1}p_{\mathrm{eff}}, \tag{6}$$

$$I\propto|p_{\mathrm{eff}}+p'_{\mathrm{eff}}|^2. \tag{7}$$

The values of the dielectric constants $\varepsilon_1(\lambda)$ and $\varepsilon_2(\lambda)$ as a function of the wavelength λ were taken from Ref. 19 as determined by the attenuated total reflection method. For the case of $d=0$, corresponding to the onset of the tunneling current in our experiments, we derive from this expression the ratio $R=I_{\mathrm{Au}}/I_{\mathrm{Ag}}$ of the SNOM signals as shown in Fig. 13. I_{Au} and I_{Ag} are the signals for a sample consisting of gold and silver, respectively. For the wavelength of 635 nm, as used in our experiments, we obtain a value of $R_{\perp}=1.162$ for a gold sphere polarized perpendicular and $R_{\parallel}=1.107$ for a gold sphere polarized parallel to the surface of the sample. A value larger than one means that a gold sample appears brighter than a silver sample. The values are in good qualitative agreement with the observed contrast, which is always on the order of 1.03 and 1.14.

However, the model accounts for neither the absolute values of the SNOM signals nor the observed approach curves. This is not surprising, considering that only a small angular range of the emitted light is detected in the SNOM experiments and that the angular distribution of the radiation depends strongly on the distance between tip and sample as is well known from experiments[8,20,21] and theory.[21,22] Our model also does not account for the absorption losses of light in the transmission through the sample.

The excited sphere of the model may possibly have its counterpart in a gold grain located on the apex of the tetrahedral tip acting simultaneously as an optical near-field and tunneling probe. Such a gold grain was indeed observed on the tip in SEM micrographs.[9] Its size could be estimated to be about 20 nm. One would suppose that the lateral resolution in SNOM images with such a grain acting as a light source should be in a first approximation equal to the size of this grain. The observed resolution in the 1-nm range, however, indicates that the interaction of the probe and the sample may be relevant in this context. The interaction of a gold sphere with a metal surface may lead to a very strong confinement of electromagnetic energy in the gap between the sphere and the sample.[23] Such an effect may be responsible for the high resolution observed at selected sites. In many images not shown here, we found that the resolution of SNOM images is generally below 10 nm and is therefore consistent with the size of a gold grain.

The contrast between silver and gold of about 8% is nearly equal to the theoretical value of the model. This indicates that most of the light emitted from the tetrahedral tip originates from a local source of dimensions comparable to the obtained resolution. A strong component of a nonlocal emission of the tip would imply a strong decrease in the contrast of local features in the image, which is not observed. We think that the local nature of our source is the main reason why we can obtain highly resolved images of a high contrast without any modulation technique for supression of nonlocal background radiation as it is necessary for SNOM configurations with nonlocal illumination of the probe.[24]

All SNOM images shown here are taken at $\lambda=635$ nm. The near-field optical contrast certainly depends on the wavelength of the illumination light. As we calculated from the quasistatic model, we expect a contrast inversion in the case of the mixed films of gold and silver at a wavelength below 516 nm for parallel and 532 nm for perpendicular polarization. This will be the subject of further spectroscopic investigations.

IV. CONCLUSION

SNOM images of mixed films of silver and gold were obtained where an edge resolution of 1 nm was obtained in image details that are not related to any measurable change in the topography of the sample. These edges in the SNOM images are accounted for by regions where a transition occurs between gold and silver being exposed at the surface of the sample. The difference in the near-field optical contrast of the more absorbing silver grains and the less absorbing gold grains is explained in terms of a quasielectrostatic model where a local light source in the form of a dipole excited gold sphere induces an image dipole in the sample that modifies the radiation from the source.

It would be very difficult to distinguish between silver and gold on a sample such as ours by a different method such as scanning tunneling spectroscopy (STS), which, for metals, is rather insensitive. SNOM with the tetrahedral tip therefore has the potential to become one of the few techniques, that are able to discriminate between different materials on a nanometer scale and have a contrast complementary to the one of STS.

We point out that no comparable resolution was obtained previously in SNOM images using light-emitting probes. Other SNOM schemes[24] in which a comparable resolution was reported use a nonlocal irradiation of the sample and the probe.

ACKNOWLEDGMENTS

We gratefully acknowledge the support by the German Science Foundation (DFG, Deutsche Forschungsgemeinschaft, Grant No. Fi-608-2) and the cooperation with the Carl Zeiss Jena GmbH. We thank R. Reichelt for high-resolution SEM investigations of the tetrahedral tips.

*Electronic address: Fischer@nwz.uni-muenster.de

[1] E. H. Synge, Philos. Mag. **6,** 356 (1928).
[2] E. A. Ash and G. Nichols, Nature **237**, 510, (1972).
[3] D. W. Pohl, W. Denk, and M. Lanz, Appl. Phys. Lett. **44**, 651 (1984).
[4] A. Lewis, M. Isaacson, A. Harootunian, and A. Muray, Ultramicroscopy **13**, 227 (1984).
[5] U. C. Fischer, J. Vac. Sci. Technol. B **3**, 386 (1985).
[6] E. Betzig, J. K. Trautman, T. D. Harris, J. S. Weiner, and R. L. Kostelak, Science **251**, 1468 (1991).
[7] U. C. Fischer, in *Near Field Optics*, edited by D. W. Pohl and D. Courjon (Kluwer Academic, Dordrecht, 1993), pp. 255–262.
[8] U. C. Fischer, J. Koglin, and H. Fuchs, J. Microsc. **176**, 281 (1994).
[9] R. Reichelt (private communication).
[10] U. C. Fischer, J. Koglin, A. Naber, A. Raschewski, R. Tiemann, and H. Fuchs, in *Quantum Optics of Confined Systems*, edited by M. Ducloy and D. Bloch (Kluwer Academic, Dordrecht, 1996), pp. 309–326.
[11] J. Koglin, U. C. Fischer, and H. Fuchs, J. Biomed. Opt. **1**, 75 (1996).
[12] U. C. Fischer and H. P. Zingsheim, J. Vac. Sci. Technol. B **19**, 881 (1981).
[13] D.-Ch. Neugebauer and H. P. Zingsheim, J. Mol. Biol. **123**, 235 (1978).
[14] H. Kuhn, J. Chem. Phys. **53**, 101 (1970).
[15] U. C. Fischer, in *Scanning Tunneling Microscopy and Related Methods*, edited by R. J. Behm, N. Garcia, and H. Rohrer (Kluwer Academic, Dordrecht, 1990), pp. 475–496.
[16] J. Koglin, Ph.D. thesis, Westfälische Wilhelms-Universität Münster (Shaker-Verlag, Aachen, 1996).
[17] R. Ruppin, Surf. Sci. **58**, 550 (1976).
[18] R. Ruppin, Surf. Sci. **127**, 108 (1983).
[19] H. Raether, in *Surface Plasmons on Smooth and Rough Surfaces and on Gratings*, edited by G. Höhler, Springer Tracts in Modern Physics Vol. 111 (Springer-Verlag, Berlin, 1988).
[20] B. Hecht, D. W. Pohl, H. Heinzelmann, and L. Novotny, in *Photons and Local Probes*, edited by O. Marti and R. Möller (Kluwer Academic, Dordrecht, 1995), pp. 93–107.
[21] C. K. Carniglia, L. Mandel, and K. H. Drexhage, J. Opt. Soc. Am. **62**, 479 (1972).
[22] A. Dereux and D. W. Pohl, in *Near Field Optics* (Ref. 7), pp. 189–198.
[23] H. Metiu, Prog. Surf. Sci. **17**, 223 (1984).
[24] F. Zenhausern, Y. Martin, and H. K. Wickramasinghe, Science **269**, 1083 (1995).